Canadian Arctic Archipelago shelf-ocean interactions: a major iron source to Pacific derived waters transiting to the Atlantic

Manuel Colombo [1,†], Birgit Rogalla [1], Jingxuan Li [1,†], Susan E. Allen [1], Kristin J. Orians [1], Maria T. Maldonado [1]

[a] Department of Earth, Ocean, and Atmospheric Sciences, University of British Columbia, BC, V6T 1Z4, Canada
Corresponding author: *Email: manuel.colombo@alumni.ubc.ca*
† Current Address: Department of Marine Chemistry and Geochemistry, Woods Hole Oceanographic Institution, 360 Woods Hole Road, Woods Hole, MA 02543-1543, USA

Highlights:

- The evolution of the Fe signature in Pacific-derived waters transiting the Canadian Arctic Archipelago (CAA) was studied.
- Arctic waters advected from the Canada Basin to Baffin Bay are enriched with iron as they transit through CAA.
- Iron enrichment in transiting Arctic Waters is driven by strong sediment resuspension events in the shallow CAA.
- Lithogenic sources dominate Fe distributions.
- Iron-rich Arctic Waters represent a dominant source of this micronutrient to Baffin Bay waters.

Abstract

Continental shelves are important sources of iron (Fe) in the land-dominated Arctic Ocean. To understand the export of Fe from the Arctic to Baffin Bay (BB) and the North Atlantic, we studied the alteration of the Fe signature in waters transiting the Canadian Arctic Archipelago (CAA). During its transit through the CAA, inflowing Arctic Waters from the Canada Basin become enriched in Fe as result of strong sediment resuspension and enhanced sediment-water interactions (non-reductive dissolution). These high Fe waters are exported to BB, where approximately 10.7 kt of Fe are delivered yearly from Lancaster Sound. Furthermore, if the two remaining main CAA pathways (Jones Sound and Nares Strait) are included, this shelf environment would be a dominant source term of Fe (dFe + pFe: 26-90 kt y^{-1}) to Baffin Bay. The conservative Fe flux estimate (26 kt y^{-1}) is 1.7 to 38 times greater than atmospheric inputs, and may be crucial in supporting primary production and nitrogen fixation in BB and beyond.

Keywords: Iron distributions, Sediment resuspension, Iron export, Trace metal biogeochemistry, Canadian Arctic Ocean, GEOTRACES

1. Introduction

Shallow coastal environments and shelf seas, key regions where seawater undergoes significant trace metal alterations, are increasingly recognized as important sources of micronutrients and trace elements to ocean waters (Homoky et al., 2016; Jeandel & Oelkers, 2015; Kipp et al., 2018; Milne et al., 2017; Morton et al., 2019). One such micronutrient, iron (Fe), regulates the nitrogen fixation and biological productivity of global oceans, and hence the marine carbon cycle (Boyd & Ellwood, 2010; Bruland et al., 1991; Moore et al., 2009). As a result, the release of Fe from the sediment-water interface and its offshore transport have been extensively investigated worldwide (Cheize et al., 2019; Cullen et al., 2009; Hatta et al., 2015; Johnson et al., 1999; Klunder et al., 2012; Lam & Bishop, 2008; Milne et al., 2017; Vieira et al., 2019). Reductive dissolution of Fe in oxygen-deficient continental sediments has long been documented as the dominant input mechanism of dissolved species of Fe at the sediment-water interface (Burdige, 1993; Elrod et al., 2004; Severmann et al., 2010). However, more recently, non-reductive sedimentary dissolution has been proposed as a major source of dissolved Fe (Abadie et al., 2017; Conway & John, 2014; Homoky et al., 2016; Jeandel & Oelkers, 2015; Pérez-Tribouillier et al., 2020; Radic et al., 2011).

The Arctic Ocean (AO) is uniquely characterized by extensive continental shelves, which comprise over half of its total area (Jakobsson, 2002), and make this enclosed ocean an ideal place to study shelf-related processes that modulate trace metal cycling and their offshore transport (Carmack & Wassmann, 2006; Charette et al., 2020; Hioki et al., 2014; Kipp et al., 2018; Klunder et al., 2012). Among the AO shelf settings, the Chukchi Sea and the Canadian Arctic Archipelago (CAA) are pathways through which Pacific-derived waters and their properties enter the AO and are exported to the North Atlantic (Beszczynska-Möller et al., 2011; Christine Michel et al., 2015). The flow of low salinity water from the Pacific Ocean ($S < 33$; Woodgate et al., 2005) to the Arctic Ocean, and to the North Atlantic, influences global thermohaline circulation (Melling et al., 2012). Pacific-derived waters also have profound effects on primary production, as these waters carry elevated macronutrient concentrations (e.g. phosphate and silicate), which fuel spring blooms in the shallow Chukchi Sea, and in the offshore Baffin Bay and Labrador

Sea domains (Carmack & Wassmann, 2006; Lehmann et al., 2019; Christine Michel et al., 2015; Varela et al., 2013). In addition to the high nutrient load advected from the Subarctic Pacific, Pacific-derived waters entering the AO are enriched in micronutrients and other trace elements (e.g. Fe and Mn) as a result of enhanced shelf-water interactions during their transit over the shallow Chukchi shelf (Aguilar-Islas et al., 2013; Kondo et al., 2016; Vieira et al., 2019).

In recent years, numerous studies in the Chukchi Sea have advanced our knowledge of the distribution of dissolved and particulate Fe, and of many other trace elements, their biogeochemistry and advection to the AO interior (Aguilar-Islas et al., 2013; Hioki et al., 2014; Jensen et al., 2020; Kondo et al., 2016; Vieira et al., 2019; Xiang & Lam, 2020). Moreover, the specific mechanisms by which Chukchi waters acquire their high Fe signature from reductive benthic sources have been recently elucidated (Jensen et al., 2020; Vieira et al., 2019; Xiang & Lam, 2020). However, the distribution and cycling of Fe in the Canadian Arctic Archipelago (CAA) remains under-studied, even though the CAA constitutes one of the largest Arctic shallow shelves and is a key export pathway of Arctic Waters (AW) of Pacific origin to the north Atlantic Ocean (Beszczynska-Möller et al., 2011; Christine Michel et al., 2015). As the AW flows through the CAA, its geochemical composition is altered due to interactions with extensive continental shelves and riverine inputs, enhancing the marine productivity downstream of the archipelago (Hill et al., 2013; Lehmann et al., 2019; Christine Michel et al., 2015; Varela et al., 2013).

This work integrates previously published dissolved Fe data (Colombo et al., 2020) in the CAA, with new measurements of particulate Fe, Al, V and Mn, as well as estimates of the prevalence of sediment resuspension from beam transmissometry data and tidal stresses, to investigate the evolution of the Fe signature in AW transiting the CAA on its journey to Baffin Bay (BB) and the Labrador Sea (LS). Additionally, this study provides insights into the mechanisms that modulate the distribution of Fe in the CAA, and the important role of shelf-water interactions as sources of this element to subsurface waters in this shallow environment, processes that differ from those postulated for the Chukchi Sea. Finally, the outflow of Fe from the CAA to BB and LS has been estimated, highlighting the significance of the

Archipelago as a source term of this essential micronutrient which can limit phytoplankton blooms in oceanic waters (Bruland et al., 2001; Schlosser et al., 2018), and potentially in BB, LS and the Subarctic Atlantic (Colombo et al., 2020; Nielsdóttir et al., 2009; Ryan-Keogh et al., 2013).

2. Study area

The Canadian Arctic Archipelago (CAA) is a complex network of islands and shallow straits that connect the Arctic Ocean to Baffin Bay (Figure 1). This shelf dominated region is an important export conduit for fresh and nutrient rich Pacific waters (high in phosphate and silicate) to the North Atlantic, enhancing the productivity downstream (Beszczynska-Möller et al., 2011; Hill et al., 2013; Michel et al., 2006; Wang et al., 2012). The CAA connects the Arctic Ocean to Baffin Bay through three main pathways: Parry Channel (sill depth ~120 m), Nares Strait (sill depth ~220 m) and Jones Sound (sill depth ~125 m; Figure 1). Within the CAA, two main domains are recognized based on conductivity, temperature and depth (CTD) data. The cooler ($-1.6 < \theta < 0.8$ °C) and fresher ($25.1 < S < 34.8$) Arctic Waters (AW) of Pacific origin dominate the western CAA (CB1 and CAA8), Penny Strait (CAA9) and the southern side of Parry Channel (CAA4 and CAA7), while Baffin Bay waters of Atlantic origin ($-1.5 < \theta < 4.9$ °C; $28.2 < S < 34.5$) recirculate on the northern side of Parry Channel (CAA1, CAA5 and CAA6; Figure 2). Station CAA3, located in southern Lancaster Sound, captures both the AW and recirculating Baffin waters (Figure 2).

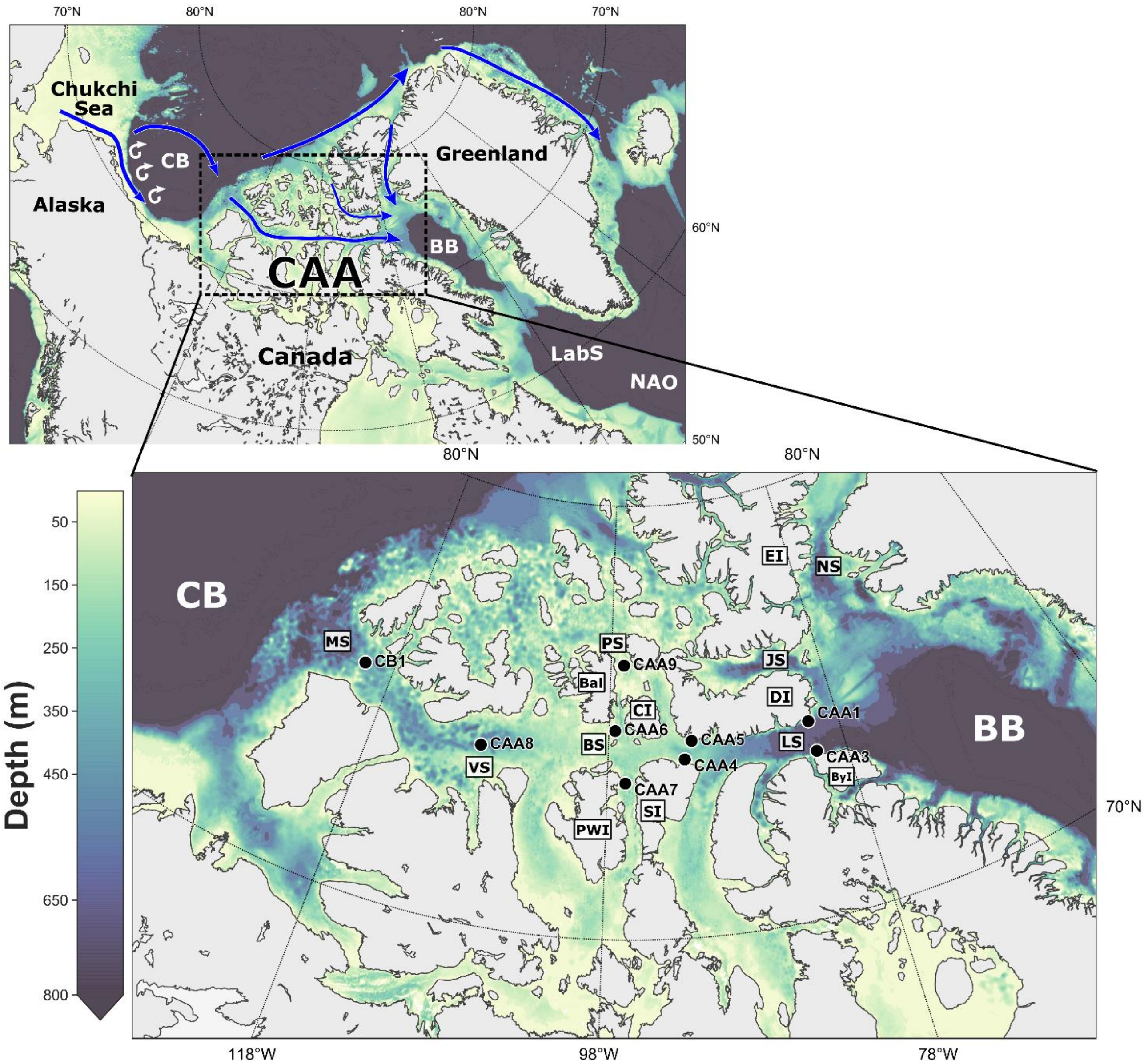

Figure 1 Stations sampled in the Canadian Arctic Archipelago (CAA) during the Canadian Arctic GEOTRACES cruises (GN02 and GN03) with bathymetry and a schematic illustration of Pacific-derived Arctic water circulation in the Canada Basin (after Aksenov et al., 2011 and Kondo et al., 2016) and the CAA (after Wang et al., 2012). A detailed view of the CAA circulation is presented in Figure 3a. Place names frequently mentioned are labelled in the expanded panel. CB: Canada Basin, BB: Baffin Bay, LabS: Labrador Sea, NAO: North Atlantic Ocean, MS: M'Clure Strait, VS: Viscount Melville Sound, BS: Barrow Strait, PS: Penny Strait, LS: Lancaster Sound, BaI: Bathurst Island, CI: Cornwallis Island, SI: Somerset Island, PWI: Prince of Wales Island, DI: Devon Island, ByI: Bylot Island, EI: Ellesmere Island, NS: Nares Strait, JS: Jones Sound. Parry Channel is the main pathway in central CAA connecting M'Clure Strait with Lancaster Sound.

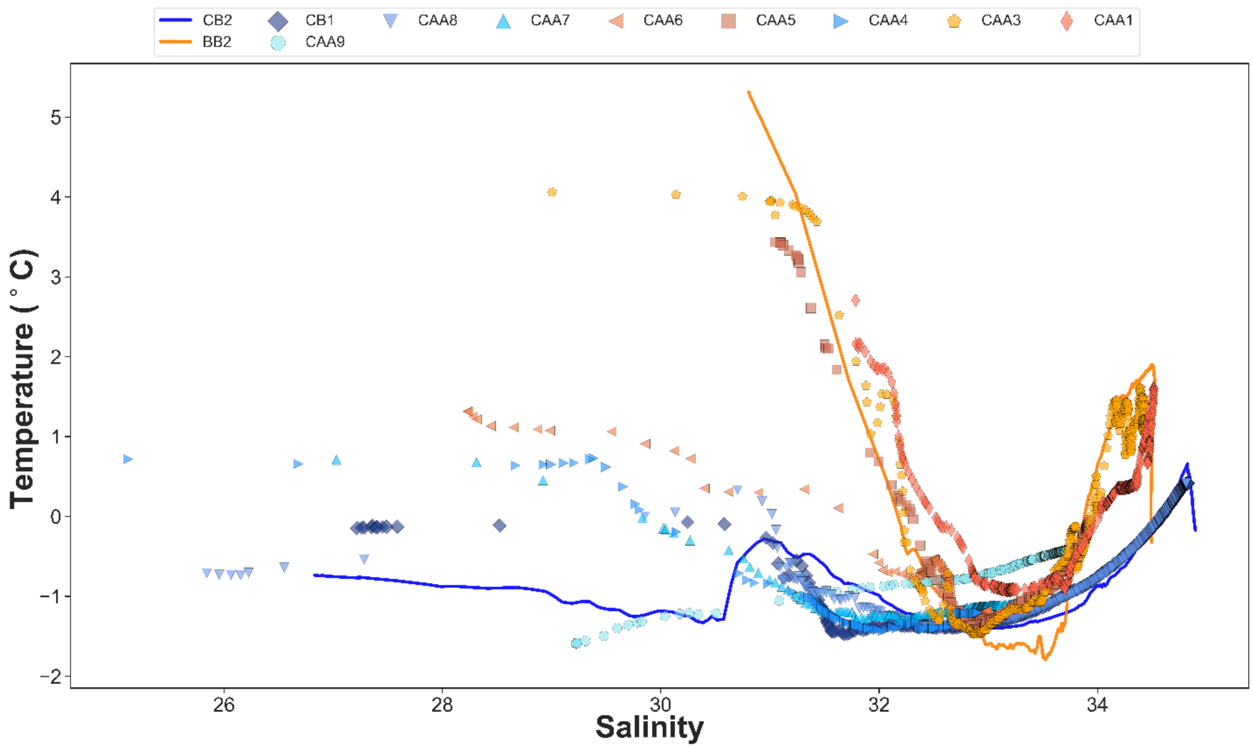

Figure 2 Potential temperature (θ) and salinity (S) for sampled stations in the CAA. Stations influenced by Baffin Waters (carrying an Atlantic signature) are displayed with orange colors, while the stations influenced by Arctic Waters (AW) are displayed in blue. The θ/S data from the Canada Basin (CB2) and Baffin Bay end-members (BB2) are shown with blue and orange solid lines, respectively.

3. Materials and Methods

3.1. Particulate trace metal sample collection

Samples were collected on the *CCGS Amundsen* as part of GEOTRACES sections GN02 and GN03 (July 10th 2015 – October 1st 2015) in the Canadian Arctic Ocean (Figure 1). The sampling was carried out during summer and early fall, and hence, most stations were ice-free when seawater samples were collected (Colombo et al., 2020). Trace metal vertical profiles ranging from approximately 10 to 600 m depth were obtained at nine stations in the CAA (Figure 1). The trace-metal clean sampling system employed to collect seawater samples consisted of a powder-coated aluminum frame with twelve 12 L Teflon-coated GO-FLO bottles (General Oceanics, Miami FL USA) and a Sea-Bird 911 CTD/SBE 43 oxygen sensor instrument package (Seabird Electronics Inc, Bellevue WA USA), attached by a 4000 m 4-member conducting Vectran cable encased in polyurethane (Cortland Cable Co., Cortland NY USA).

Onboard the ship, samples were transferred to a trace metal clean sampling van (HEPA filtered environment), where ten liters of unfiltered seawater were collected into pre-cleaned 10 L LDPE cubitainers (Bel Art and Nalgene) with a piece of C-flex tubing (Masterflex) and a Teflon straw. Seawater was filtered inside a HEPA-filtered clean air bubble using 0.45 µm Supor filter (47 mm diameter) and an assembled filtration system (a cubitainer, a spigot, C-flex tubing, a peristaltic Cole-Parmer pump, a 47 mm Millipore filter holder with customized screws, waste tubing and a waste container for volume recording). After filtration, the filters were dried inside a laminar flow hood, folded in half, and stored in clean poly bags until analysis. Supor filters were always handled using pre-cleaned forceps and clean gloves. The sampling devices, containers and the filtration system were cleaned according to GEOTRACES protocols (https://www.geotraces.org/).

3.2. Sample processing and analysis

In order to prevent contamination, the processing and analysis of particulate trace metals was conducted at the University of British Columbia (UBC) in class 1000 laboratories, pressurized with HEPA filtered air and under class 100 laminar flow fume hoods. All the plasticware used during the sample preparation and analysis were cleaned according to GEOTRACES protocols.

Filters containing the particulate fraction were processed at UBC following the protocol described by Ohnemus et al. (2014) and Li (2017). In brief, the organic fraction and the Supor filters were digested by heating the filters (110 °C for 60–120 min) in Teflon flat-bottom Savillex vials containing sulfuric acid/hydrogen peroxide (H_2SO_4/H_2O_2; 3:1). Then, the mineral matrix residues were heated and digested under reflux (3-4 h at 100-110 °C) using a mixture of HNO_3, hydrochloric acid (HCl) and hydrofluoric acid (HF). After taken to dryness, 2 mL of HNO_3/H_2O_2 [1:1] were added to each vial and dried for a second time on a hotplate at 100-110 °C. The dry residues were resuspended in a small volume (100 μL) of HNO_3, heated at 110 °C and then dried at 135 °C. Finally, the clear residues were resuspended in 1% HNO_3 with 10 ppb of indium as an internal standard; particulate samples were diluted prior to ICP-MS analysis. All reagents used in the digestion and subsequent sample preparation (H_2SO_4, HNO_3, HCl, HF and H_2O_2) were Optima grade (Fisher Scientific, Ontario, Canada).

Particulate Fe, Al, V and Mn were analyzed from a twelve-point calibration curve prepared in 1% trace metal grade HNO_3 from 1 ppm certified single element standards. The analyses were conducted by a high resolution Thermo Finnigan Element2 ICP-MS at the Pacific Centre for Isotopic and Geochemical Research (PCIGR) at UBC. A medium mass resolution was selected for Fe, V and Mn in order to remove isobaric interferences, and Al was analyzed using low mass resolution. During sample analysis, solution blanks (1% HNO_3 Milli-q water with indium) and filter blanks were run to ensure quality throughout the measurements; particulate trace metal concentrations reported here were corrected for the analytical blank by subtracting the average solution blank on the corresponding analytical day and from the filter blank measurements. The accuracy and precision of this method was tested by analyzing the certified reference material BCR-414 and GEOTRACES inter-calibration samples collected in the Pacific Ocean, which underwent the same digestion and analytical method described above. Measured values in this study are in good agreement with consensus values (mean, standard deviation, relative standard deviation and solution and filter blank concentrations are listed in Table S1in the supporting information document).

3.3. Sediment resuspension estimates, water transport fluxes and statistical analysis

To understand the prevalence of resuspension within the CAA, we (1) identify individual sediment resuspension events from CTD transmissivity profiles and (2) estimate the integrated effect of resuspension over time based on tidal stresses. Below, we explain these two approaches.

For the sediment resuspension events, we examined more than 1400 CTD transmissivity observations measured on ArcticNet cruises between 2006 and 2018 using a Sea-Bird SBE-9plus CTD with a Wetlabs C-Star transmissometer (Table S2). The data are sourced from publicly available measurements from ArcticNet, a Network of Centres of Excellence of Canada, accessed through the Polar Data Catalogue (https://www.polardata.ca/). From all available profiles, we focused on profiles that reach within 30 m of the sea floor and that are deeper than 75 m total depth (463 profiles satisfied this requirement; locations and profiles in Figure S1) to capture the near-bottom effect of resuspension. With these profiles, we calculated a "transmissivity drop" metric by subtracting the average transmissivity in the bottom 5 m of each profile from the average of the 80 m above, to account for background transmissivity. We exclude measurements from the upper 60 m of the water column in order to omit transmissivity changes related to primary production, i.e. increased organic particle export. A strong decrease in transmissivity near the bottom, indicates that the transmissivity profile captured a resuspension event at that CTD cast location. Tidal flow over topography can generate sediment resuspension, hence, we can estimate the integrated prevalence of sediment resuspension in the CAA as proportional to the tidal stress, or barotropic tidal speed squared (Wang, 2002).The barotropic tidal speeds were extracted and interpolated by Epstein (2018) from the MOG2D-G hydrodynamic gravity waves model (Carrère & Lyard, 2003). It is worth considering that significant seasonal tidal variation, linked to wintertime sea-ice cover, has been recently described in the

CAA (Rotermund et al., 2021). In the Kitikmeot region (southern CAA), the damping may account for up to a 50% reduction of tidal amplitude, while a moderate tidal reduction is modeled in western CAA (20-30%). Nonetheless, in the rest of the CAA (i.e. eastern Parry Chanel, Nares Strait) tidal damping is small to negligible (10% at most; Rotermund et al., 2021).

The Fe export from the CAA to BB across Lancaster Sound, Jones Sound and Nares Strait boundaries was calculated for the upper 50 m of the water column and below using five-day averaged velocity fields from 2002 to 2019, a time frame which encompasses the sampling dates. The velocity fields originate from a 1/12 degree coupled ocean-ice model of the Arctic and Northern Hemispheric Atlantic, ANHA12, within the Nucleus for European Modeling of the Ocean, NEMO (Madec et al., 2017). ANHA12 simulates the average flow structure within the CAA well (Hughes et al., 2017) and the net volume flux estimates for Lancaster Sound (0.696 Sv), Jones Sound (0.01 Sv) and Nares Strait (0.933 Sv) agree with previous modeled and observational data (Melling et al., 2008; Zhang et al., 2016). For further details of the configuration, see Hu et al. (2018) and Grivault et al. (2018). The statistical analysis and graphics in this manuscript were developed using Python 3.6.0. programming language (www.python.org/) and NumPy (numpy.org), Matplotlib (matplotlib.org) and pandas (pandas.pydata.org) libraries.

4. Results and Discussion

This study reports, for the first time, vertical and spatial distributions of particulate Fe, Al, V and Mn concentrations, along with sediment resuspension estimates in the Canadian Arctic Archipelago (CAA). The full dataset of particulate trace elements presented in this manuscript is shown in Table S3. Dissolved Fe data was retrieved from Colombo et al. (2020; Table S4). The primary aim of this study is to investigate the evolution of the Fe signature as well as other trace elements in Arctic waters (AW) transiting the CAA, and to demonstrate the important role of shelf-ocean interactions and sediment resuspension as sources of these elements in this dynamic environment.

4.1. Vertical distributions, spatial variability and sources of Fe in the shallow Canadian Arctic Archipelago

In this study, we traced transformations in the Fe signature of AW transiting from the Canada Basin (CB) to Baffin Bay (BB; Figure 3a) with nine profiles collected in the CAA. With the exception of station CAA1, vertical distributions of dFe and pFe were highly correlated (R^2= 0.70; Figure 3b), indicating that similar sources and sinks control Fe distributions in this region. Although spatially variable, vertical distributions of dissolved and particulate Fe in the CAA displayed a similar shape, with lower concentrations in surface waters, increasing with depth and peaking at the sediment-water interface (Figure 3a). Interestingly, dFe (AVG: 1.64 nmol kg^{-1} and 25/75th percentiles: 0.804-2.01 nmol kg^{-1}) and pFe (AVG: 16.7 nmol L^{-1} and 25/75th percentiles: 4.70-17.8 nmol L^{-1}) concentrations were much higher in the shallow and shelf-dominated CAA than those measured in the neighboring deep (~1000-3500 m) Canada Basin (CB), Baffin Bay (BB) and Labrador Sea (LS); approximately 100 to 250% and 90 to 1000% higher for dFe and pFe (Colombo et al., 2020; Li, 2017).

Freshwater inputs are driving the distinctively high CAA Fe signature. In the CAA, small permafrost draining rivers and glacially fed streams are common, and their combined outflow delivers 201 to 257 km^3 yr^{-1} of freshwater (Alkire et al., 2017) along with a high load of dissolved and particulate elements. For some elements, such as Fe, their riverine concentrations are many times greater than those in transiting AW (Colombo et al., 2019). These augmented freshwater sources in the CAA –including land fast sea ice melt–, likely explain the high dFe concentrations (AVG±SD: 0.939±0.368 nmol kg^{-1}; Figure 3a) measured in surface waters ($d < 40$ m), compared with deeper Canadian Arctic basins such as the CB, BB and the LS (Colombo et al., 2020). Similarly, pFe concentrations in the upper ten meters (8.60±2.93 nmol L^{-1}, excluding the extremely high concentrations measured in near-surface waters at CB1 and CAA3; Figure 3a) were significantly higher than CB, BB and LS surface waters (Li, 2017).

Increased shelf-water interactions and sediment resuspension drive the substantially higher subsurface Fe concentrations measured in the shallow (d < 650 m; Figure 1) CAA compared with incoming AW from CB. Dissolved and particulate Fe concentrations increased with depth from about 50 m (σ_θ> 25.50), reaching the highest concentrations, for most CAA stations, close to the sediment-water interface. However, a marked spatial difference in Fe distributions was observed between stations located in the western region (CB1 and CAA8) and those located east of Barrow Strait (CAA1, CAA3-CAA7 and CAA9; Figure 3a). In the western CAA, subsurface concentrations moderately increased with depth at station CB1 (dFe Min-Max range: 0.688-1.10 nmol kg^{-1}; pFe: 1.53-9.19 nmol L^{-1}) and CAA8 (dFe: 0.447-1.15 nmol kg^{-1}; pFe: 1.69-6.48 nmol L^{-1}), displaying a slight increase in near-bottom waters. On the other hand, much higher subsurface concentrations were measured in the central sills area of Parry Channel (d < 200 m), near Barrow Strait (confined by Bathurst, Cornwallis, Devon, Sommerset and Prince of Wales Islands; Figures 1 and 3a). In this shallow area (stations CAA4-CAA7), dFe and pFe sharply rose with depth below 50 m, peaking at the sediment-water interface (dFe: 2.01-5.13 nmol kg^{-1}; pFe: 16.0-78.9 nmol L^{-1}), with values that were from 100 to 900% greater than those of the western CAA. This high Fe signature was advected to the Lancaster Sound, where station CAA3 captures the AW outflow before entering BB. Although the magnitude was reduced, subsurface Fe concentrations (dFe: 0.750-2.24 nmol kg^{-1}; pFe: 1.72-13.0 nmol L^{-1}) were still higher at CAA3 than those of the western CAA (Figure 3a).

In addition to the general trends highlighted above, the vertical distribution of Fe in Penny Strait (station CAA9) and in northern Lancaster Sound (station CAA1) exhibited noteworthy features. A subsurface glacial plume (discussed in section 4.4) was observed at station CAA1, extending from approximately 30 to 200 m (σ_θ = 25.92-27.15; Figures 3a and 4). In Penny Strait (CAA9), subsurface concentrations were within the range of the eastern CAA stations (Figures 3a and 4), but the near-bottom Fe maximum described for aforementioned stations was smoothed. The lack of a near-bottom Fe peak is most likely attributed to the strong tidal mixing in Penny Strait, which is also reflected in the near linearity of the temperature and salinity profiles (Figure 2).

The sources (e.g. lithogenic, biogenic, authigenic) of pFe in the CAA were elucidated by normalizing pFe to pAl, and comparing this ratio to the average upper continental crustal (UCC) ratios (Rudnick & Gao, 2013; Shaw et al., 2008). Particulate Al has been extensively used as a lithogenic tracer due to its high natural abundance in the earth's crust and similar concentration range in both the UCC and bulk continental crust, the relatively constant ratio of metal to aluminum in crustal rocks, and its scarce anthropogenic sources (Covelli & Fontolan, 1997; Lee et al., 2018; Ohnemus & Lam, 2015).

Particulate Fe to particulate Al showed a very strong positive correlation (R^2 = 0.96) across many orders of magnitude, with a ratio (0.179) that agrees well with those reported for the UCC. This correlation evidences the overwhelming dominance of lithogenic-derived inputs (100 %; estimated as $\%pFe_{litho} = 100x\left(\frac{pAl}{pFe}\right)_{sample} x\left(\frac{pFe}{pAl}\right)_{UCC}$) of pFe in the CAA (Figures 3c and S2). No significant correlation (R^2 < 0.01 / *p-value* > 0.05) was found between pFe and pP, which indicates that phytoplankton biomass does not contribute substantially to the pFe pool. Therefore, the biogenic component of pFe –the most abundant trace metal in phytoplankton– is completely masked by its lithogenic fraction in this land-dominated ocean environment (Figure 3c and S2).

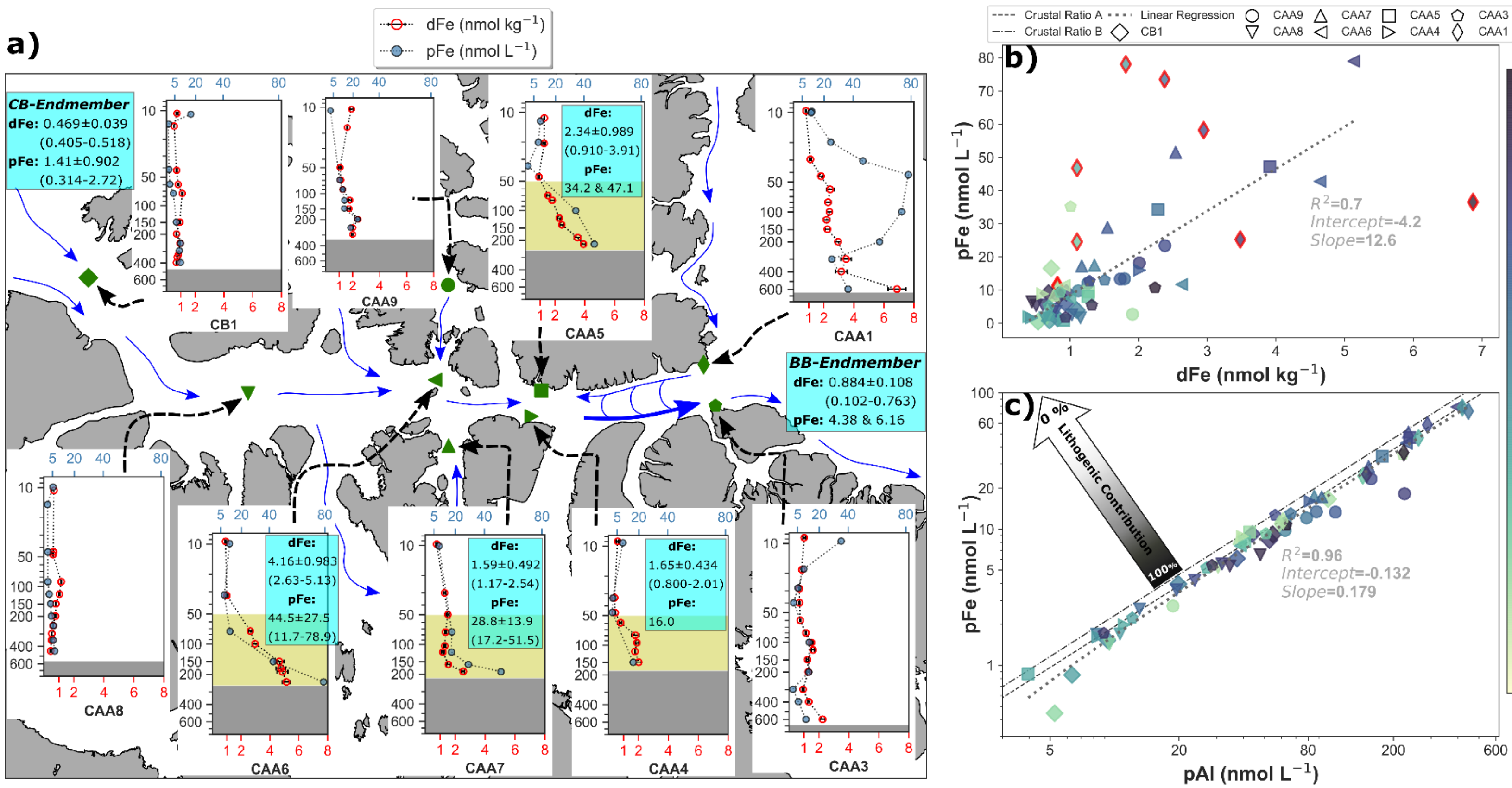

Figure 3 (a) Vertical distributions of dissolved and particulate Fe (dFe and pFe) sampled in the CAA; dFe data was retrieved from Colombo et al. (2020). The gray shading in each profile indicates the seafloor, and the pale green shaded area in the central sills region (stations CAA4-CAA7) indicates those samples below 50 m, where concentrations sharply increased with depth (AVG±SD as well as ranges of dFe and pFe in subsurface waters for these stations are displayed in the light blue boxes). Concentrations of dFe and pFe measured in inflowing subsurface Arctic-derived waters in the Canada Basin shelf-break (CB-Endmember; σ_θ = 25.30-27.95) and from the Baffin Bay slope region capturing the Arctic Water outflow (BB-Endmember; σ_θ = 26.30-27.12) were retrieved from Colombo et al. (2020) and Li (2017). Circulation pathways in the CAA are indicated by blue arrows (after Michel et al. 2006 and Wang et al., 2012). (b) Relationship between pFe and dFe in the CAA; samples from station CAA1 (red edged diamonds) were excluded from the linear regression due to the presence of massive glacial inputs at this station (discussed below). (c) Relationship between pFe versus pAl in the CAA; note the logarithmic scale of the plot. Depth values for each analyzed sample are displayed with the color scale. The lines displayed on this figure indicate a linear regression fit (gray dotted line), and the average upper continental crustal (UCC) ratios (dash-dotted & dashed lines). UCC pFe to pAl molar ratios of the Canadian surface Precambrian shield (crustal ratio A) were selected from Shaw et al. (2008), and from an updated continental crust composition review (crustal ratio B; Rudnick and Gao, 2013). Samples plotting along the crustal ratios are assumed to be lithogenically derived (lithogenic contribution arrow); in the CAA, no samples plotted above the crustal ratio B.

4.2. The importance of shelf-ocean interactions and sediment resuspension for the distribution of Fe, as well as pAl, pV and pMn

Increased shelf-ocean interactions in the CAA not only control the distributions of dFe and pFe, but also those of pAl, pV and pMn. In this study, significantly higher concentrations of pAl (AVG: 93.9 nmol L^{-1} and 25/75th percentiles: 25.2-125 nmol L^{-1}) and pV (AVG: 91.3 pmol L^{-1} and 25/75th percentiles: 37.0-114 pmol L^{-1}) were measured in the CAA (Figure 4) compared to the deep (~1000-3500 m) Canada Basin, Baffin Bay and Labrador Sea (190-700% and 70-230% higher for pAl and pV; Li, 2017). Notwithstanding, pMn concentrations in the CAA (AVG: 926 pmol L^{-1} and 25/75th percentiles: 289-1091 pmol L^{-1}) were similar to those measured in the deep Canada Basin and Baffin Bay (Li, 2017), as further discussed below. Overall, pV and pAl were well correlated across the CAA ($R^2 = 0.82$) and their ratio (0.00068) was within the range of the UCC ratios (Figure S2), while pMn:pAl ratios were not correlated ($R^2 = 0.12$) and markedly deviated from the UCC ratio (Figure S2). Subsurface ($\sigma_\theta > 25.50$) concentrations of particulate Al, V and Mn also increased with depth to the seafloor, exhibiting the same spatial variability described for Fe. Near-bottom samples in the central sills area were highly enriched in pAl (81.6-395 nmol L^{-1}), pV (81.3-442 pmol L^{-1}) and pMn (1091-4035 pmol L^{-1}), with values up to 500% (pMn) to 700% (pAl and pV) higher than concentrations measured in western CAA near-bottom samples (Figure 4).

The geographical and hydrological CAA setting (a shallow region with extensive shelves, where mixing is ubiquitous and favors shelf-water interactions) enhances the Fe pool (dissolved and particulate) of AW transiting from the Canada Basin to Baffin Bay (Figure 3a). Mixing is not uniform across the CAA; it is particularly strong in the central sills area (d < 200 m; Figure 1) as a result of tidal forcing, shear instabilities and the breaking of internal waves over the rough topography. Averaged diapycnal diffusivities and buoyancy fluxes in the central sills area are up to an order of magnitude larger than in the western CAA (Hughes et al., 2017). The energetic interaction of currents with bottom topography results in intense sediment resuspension events, which are reflected in transmissivity drops and the concomitant maxima of pFe and dFe –as well as other trace metals– near sediment-ocean boundaries, especially in the Barrow Strait area (stations CAA4-CAA7; Figures 3a and 4). In order to explore the extent and spatial variability of sediment resuspension events in the CAA, we determined the near-bottom transmissivity drop and looked at the tidal stress in this region (section 3.3).

Spatial trends from the transmissivity drop metric, calculated from more than 450 observations available for the Canadian Arctic Ocean (Figure S1 and Table S2), agree well with the distribution of tidal stress magnitudes in the CAA (Figure 5). In the tranquil western CAA region, from M'Clure Strait to Viscount Melville Sound, tidal stresses (< 0.0008 m^2 s^{-2}) and transmissivity drop values (~ 1 %) were considerably lower than in the eastern CAA (tidal stress ~0.0030-0.030 m^2 s^{-2} and transmissivity drop values up to 5 %; Figure 5), features which are linked with dFe, pFe, pAl, pV and pMn distributions (lower concentrations in the western vs. eastern CAA; Figures 3a and 4). Indeed, the highest tidal stresses and largest transmissivity drops occurred in the central sills area of the CAA, surrounded by Bathurst, Cornwallis, Devon, Sommerset and Prince of Wales Islands (Figure 5), where mixing is enhanced (Hughes et al., 2017), and the highest dFe and pFe were measured (stations CAA4-CAA7, Figure 3a).

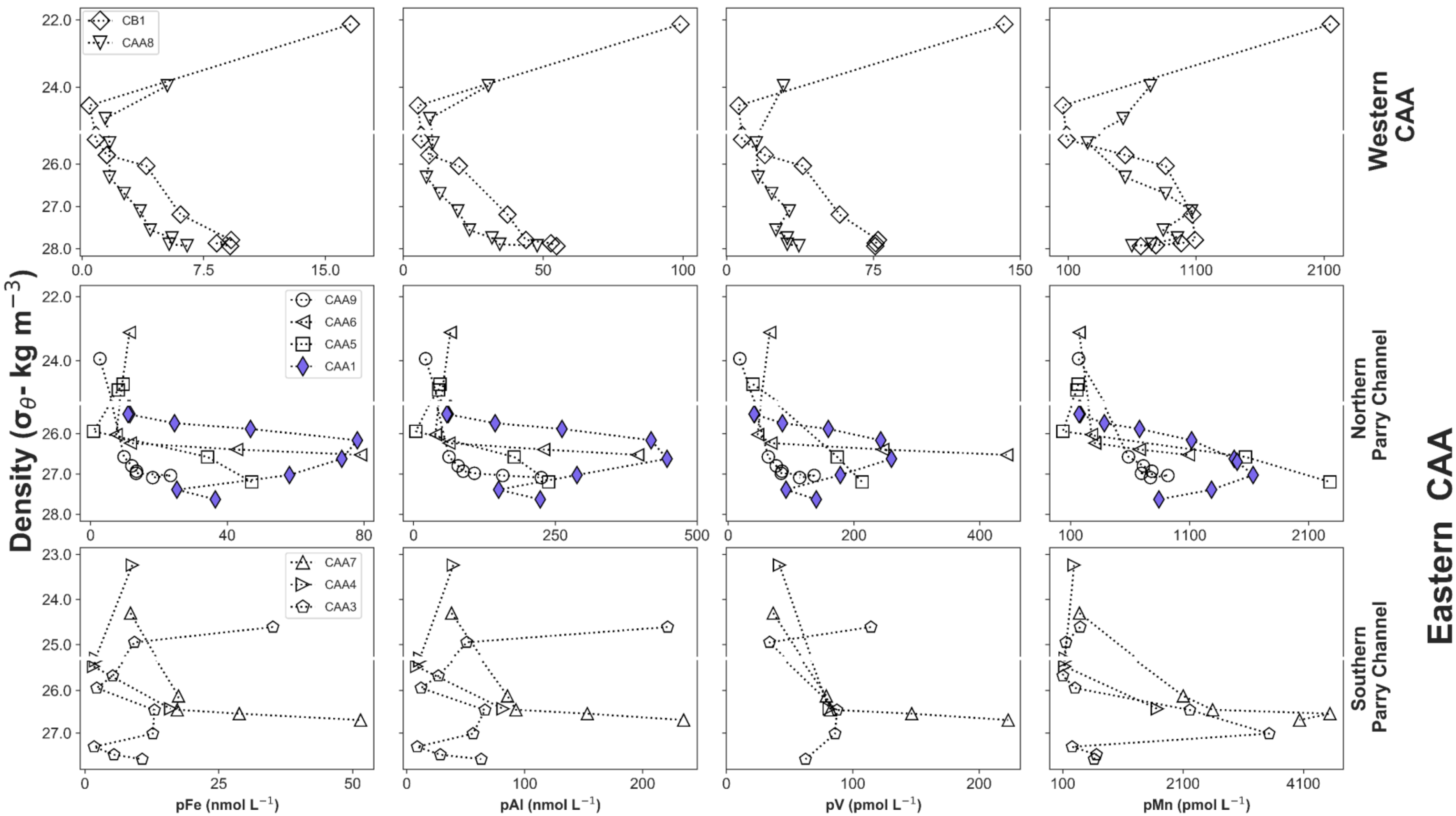

Figure 4. Profiles of particulate Fe, Al, V and Mn versus potential density (σ_θ) in the Canadian Arctic Archipelago (CAA). Upper panel: western CAA stations (CB1 and CAA8), middle panel: stations located in Northern Parry Channel (CAA1, CAA5-6 and CAA9), bottom panel: stations located in Southern Parry Channel. Particulate profiles from CAA1 are shown in blue to highlight the presence of a subsurface glacial plume influencing this station. Note that the magnitude of particulate trace metal concentrations (x-axes) vary among the plots.

Particulate trace metal concentrations shed light on the mechanisms driving the increase of dFe and pFe in CAA waters and their maximum at the sediment-water interface, unveiling a large difference in the supply of this element between the CAA (non-reductive dissolution) and the Chukchi Sea (reductive dissolution). These two regions are main gateways for relatively fresh Pacific-derived waters transiting from the North Subarctic Pacific to the North Subarctic Atlantic (Beszczynska-Möller et al., 2011). Both the CAA and the Chukchi Sea are characterized by extensive and shallow shelves, with enhanced shelf-water interactions which greatly modify the Fe signature of transiting waters (Jensen et al., 2020; Vieira et al., 2019; Xiang & Lam, 2020). However, distinct biogeochemical processes explain the dFe and pFe increase with depth and the near-bottom maxima in the shallow Chukchi and CAA shelves (Figure 6).

In the Chukchi Sea, large pulses of organic matter trigger strong reducing conditions in sediments, where Fe and Mn oxides undergo reductive dissolution; reduced species (Fe^{+2} and Mn^{+2}) then diffuse to overlying oxygenated bottom waters (Vieira et al., 2019). Given the faster oxidation kinetics of Fe^{+2} than Mn^{+2} in overlying waters, dFe is rapidly oxidized and precipitated near the shelf region, while Mn remains in the dissolved phase for longer time. The decoupled behavior of Fe and Mn leaves Chukchi Sea waters moderately enriched in dFe (up to ~20 nmol kg^{-1}) and greatly enriched in non-lithogenic pFe oxides, whereas dMn exhibits a larger spike (up to ~200 nmol kg^{-1}) and pMn oxides are virtually absent on Chukchi shelves (Jensen et al., 2020; Xiang & Lam, 2020).

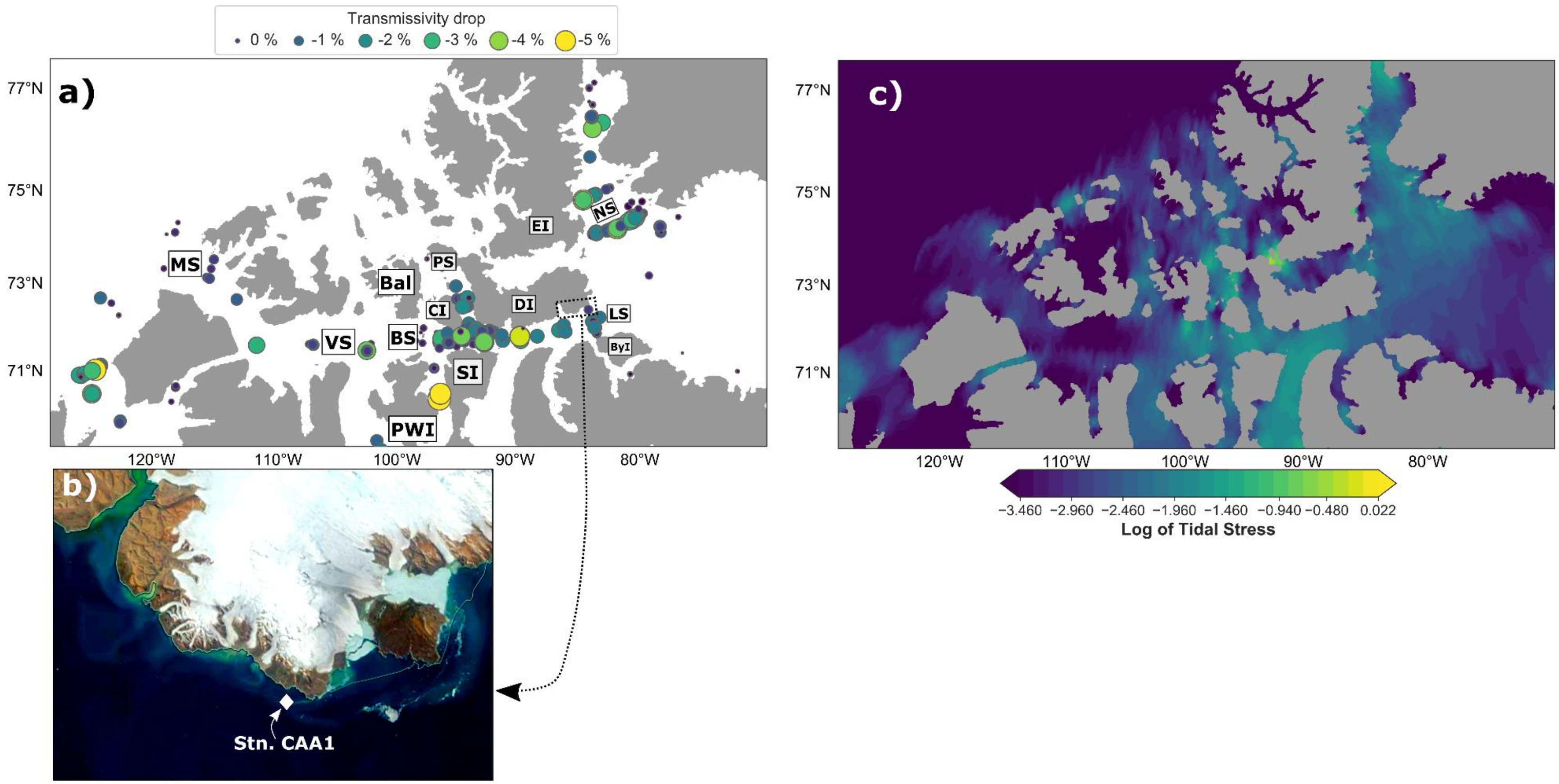

Figure 5 (a) Transmissivity drop (Methods) near the ocean floor in the Canadian Arctic Archipelago; for an expanded figure of the entire CAO, see Figure S3. Observations accessed through the Polar Data Catalogue (https://www.polardata.ca/). MS: M'Clure Strait, VS: Viscount Melville Sound, BS: Barrow Strait, PS: Penny Strait, LS: Lancaster Sound, BaI: Bathurst Island, CI: Cornwallis Island, SI: Somerset Island, PWI: Prince of Wales Island, DI: Devon Island, ByI: Bylot Island, EI: Ellesmere Island, NS: Nares Strait. Parry Channel is the main pathway in central CAA connecting M'Clure Strait with Lancaster Sound. (b) Terra-MODIS visible image of eastern Devon Island taken on Jul. 25, 2015 (https://worldview.earthdata.nasa.gov/), illustrating the presence of glacial runoff along the Devon Island coast, where station CAA1 is located. (c) Logarithmic plot of barotropic tidal stress interpolated from Carrère and Lyard (2003).

In the CAA, unlike the Chukchi shelves, reductive benthic supply of Fe^{+2} is not anticipated to be the dominant source of dFe to subsurface waters. Even though primary production levels in the CAA are higher than those in inflowing AW from the CB, they are substantially lower than the highly productive Chukchi Sea (Varela et al., 2013). Therefore, reduced vertical pulses of organic matter along with strong mixing regimes (Hughes et al., 2017) and sediment resuspension events (Figure 5) result in oxygenation of the seafloor (in near-bottom waters, $O_2 > 200$ µmol kg^{-1} or 4.6 ml L^{-1}), which likely weaken the reductive supply of Fe^{+2} in the CAA. In fact, N* values (a quasi-conservative tracer of nitrogen dynamics; large negative values indicate denitrification and reducing conditions within sediments) in the CAA were more positive in near-bottom waters (CB1, CAA1, CAA3, CAA5-6 and CAA8-9: -2.6 to 2.5; CAA4: -6.3; CAA7: -5.6; Figure S4) than overlying waters. These values are much higher than those measured in Chukchi Sea near-bottom waters (N* ~ -15) where strong reducing sediment conditions are present, and dFe, dMn and non-lithogenic pFe show strong negative correlations with N* (Jensen et al., 2020; Figure 6). In contrast to what has been observed in the Chukchi Sea, the pFe pool in the CAA is entirely lithogenic-dominated, and dFe, dMn and non-lithogenic pMn concentrations do not show any clear relationship with N* (Figure S4). Therefore, the lack of relationship of Fe distributions and N*, the modest increase of dFe and dMn (up to ~7 and 11 nmol kg^{-1}, respectively; Figures 3a and S4), the overwhelming dominance of lithogenic pFe (Figures 3, S2 and S4) and the strong sediment resuspension events (Figure 5), all point to non-reductive sedimentary sources (desorption / dissolution) of Fe in the CAA. Non-reductive dissolution of lithogenic material is increasingly being recognized as an important, but often underestimated, source of Fe to ocean waters in the Pacific, Atlantic and Southern oceans (Abadie et al., 2017; Conway & John, 2014; Homoky et al., 2016; Pérez-Tribouillier et al., 2020). Although no trace metal samples were collected in Jones Sound and Nares Strait during the Canadian GEOTRACES GN02 and GN03 cruises, similar processes are expected to control Fe distributions in these regions, where transmissivity drops and tidal stresses (and thus the prevalence of sediment resuspension) are comparable to those in the central sills area of the CAA (Figures 5 and S3).

Interestingly, the pMn pool in subsurface CAA waters was dominated by Mn oxides (Figure S1), with the stations located in the western CAA (CB1 and CAA8) and in southern Parry Channel (CAA3, 4 and CAA7) yielding the largest non-lithogenic fractions of pMn (> 60%). The predominance of Mn oxides is not related to benthic sources (reduction in the sediment→ diffusion to the overlying waters→ oxidation→ precipitation), but with the advection of halocline waters from the Canada Basin (CB). Recent studies found that authigenic oxidative precipitation of pMn is pervasive in CB halocline waters (non-lithogenic fraction > 97%; Li, 2017 and Xiang and Lam, 2020), which enter the CAA through M'Clure Strait (CB1), and travel eastward from Viscount Melville Sound (CAA8) to Lancaster Sound (CAA3) along the southern edge of Parry Channel (CAA4 and CAA7; Figures 1 and 2).

4.3. The downstream significance of shelf-derived Fe export to Baffin Bay and biological implications

In order to assess the significance of shelf-water interactions as a source term of Fe to AW, we estimated the Fe export from the central sills area to Lancaster Sound and from Lancaster Sound to BB using simulated net mean eastward AW outflow (section 3.3) and dissolved and particulate Fe inventories. As the eastward flow of AW of Pacific origin is restricted to the southern side of Parry Channel, dFe and pFe average concentrations measured in stations CAA4 and CAA7 were used to calculate Fe fluxes from the central sills area, and average concentrations from station CAA3 were used to calculate Fe fluxes from Lancaster Sound to BB. To account for the sharp increase in Fe concentrations with depth, Fe export fluxes have been split into an upper 50 m layer and a lower layer (> 50 m; Figure 3), multiplying the Fe inventories by the AW volume transport of these two layers (Table 1). This calculation reduces the associated biases that may arise when fluxes are calculated by multiplying the mean volume transport by the mean Fe concentration for the entire water column. Adding together the Fe fluxes from the upper and lower layers yields an annual dFe and pFe export from the central sills area into Lancaster Sound on the order of 2.9 x 10^7 moles (1.6 kt y^{-1}) and 4.1 x 10^8 moles (23 kt y^{-1}), respectively (Table 1). The annual dFe and pFe exported from Lancaster Sound into Baffin Bay is 2.6 x 10^7 moles (1.5 kt y^{-1}) and 1.7 x 10^8 moles (9.2 kt y^{-1};

Table 1). The slightly reduced Fe export values estimated from the Lancaster Sound compared with the central sills area may reflect the dilution effect resulting from the recirculation of the saltier and warmer Baffin Bay waters mixing with AW flowing eastward in Lancaster Sound (Figures 2 and 3).

In order to provide some context about the importance of Fe contributions from Lancaster Sound to BB, we compare our estimates with atmospheric inputs to BB waters. For the calculations, atmospheric Fe fluxes of 1.0 and 21.5 mg m^{-2} y^{-1} were used, as they represent the lower and upper limits measured in the western region of the Arctic Ocean and at Alert Station in the CAA (Kadko et al., 2016; Marsay et al., 2018). Based on these measurements, the annual atmospheric deposition of Fe to BB (area is 6.89 $x10^{11}$ m^2) span from 0.689 to 14.8 kt y^{-1}, values that are at the same level, or lower, than the estimated Fe export from the CAA via Lancaster Sound (Table 1). From the annual atmospheric fluxes, we calculated the fraction of Fe available for phytoplankton, using low (1.4%) and high (54%) solubility values from bulk aerosols (Baker et al., 2006; Shelley et al., 2018). The potential bioavailable Fe that can be derived from aerosols to BB waters is also in the same range, or lower, as that advected by AW from Lancaster Sound, if both the dFe and the soluble fraction of the particulate phase (assuming 1.4-54% Fe solubility; Baker et al., 2006; Shelley et al., 2018) are taken into account (Table 1). If the entire bioavailable Fe exported from Lancaster Sound (1.6-6.5 kt y^{-1}) was used by primary producers, and assuming a Fe:C ratio of 30 µmol:mol, representative of phytoplankton stoichiometry (10-50 µmol:mol; Biller and Bruland, 2014; Twining et al., 2015), the maximum carbon fixed in BB and downstream would range from 11 to 46 Tg C y^{-1} for the low and high Fe solubility values, respectively. Likewise, the maximum nitrogen fixed if all the bioavailable Fe is used by diazotrophic cyanobacteria, and assuming a Fe:C ratio of 48 µmol:mol (Berman-Frank et al., 2001; Kustka et al., 2003) and a C:N ratio of 11 mol:mol (Karl et al., 2002; Küpper et al., 2008), would range from 0.7 to 3 Tg N y^{-1}. To put the estimated ranges of carbon and nitrogen fixation presented here into perspective, the estimated annual depth-integrated primary productivity in the Labrador Sea-Baffin Bay domain is 323±117 Tg C yr^{-1} (Varela et al., 2013) and the total nitrogen fixation in the North Atlantic is about 22 Tg N yr^{-1} (Moore et al., 2009). However, as we only computed the Fe exported from Lancaster

Sound, which accounts for ~40% of the AW outflow through the CAA (Zhang et al., 2016), the overall Fe supply from CAA shelves to BB is expected to be larger. The remaining AW transiting CAA (~60%; Table 1) flows to BB through Jones Sound and Nares Strait (Figure 1), shallow shelf regions where sediment resuspension events are ubiquitous (Figure 5), and benthic Fe inputs are presumably strong as described for Parry Channel and Lancaster Sound. We conservatively estimated the Fe exported by Jones Sound and Nares Strait (regions not sampled in this study) into BB by multiplying their volume fluxes by average Fe concentration from CAA3 in Lancaster Sound, as this station captures both the Fe enriched waters transiting the archipelago and recirculating waters from BB. As the Nares Strait (NS) region is characterized by large glacierized areas along the Northern Ellesmere Island and Greenland, an upper boundary Fe flux estimate from NS (~57% of the AW outflow) was also computed by multiplying NS volume flux by average Fe concentration from CAA1 (glacial influenced station; section 4.4.). If the three main pathways are considered, the total annual Fe exported from the CAA into Baffin Bay would range from 26 kt y^{-1} (conservative estimate) to 90 kt y^{-1} (upper boundary estimate; Table 1). The conservative estimate of Fe exported from CAA shelves is almost double the maximum atmospheric Fe flux estimate to BB (Table 1), and the potential bioavailable Fe (15.7 kt; Table 1) could support up to a third of the depth-integrated primary productivity in the Labrador Sea-Baffin Bay domain.

Table 1 Net volume flux, dissolved and particulate Fe concentration (AVG±STD), yearly Fe export from the Central Sills Area, Lancaster Sound, Nares Strait and Jones Sound, and annual input of Fe to Baffin Bay (area= $6.89e^{+11}$ m^2) from atmospheric deposition and dissolution (total and bioavailable Fe) compared to Fe exported from the CAA. Dissolved Fe concentrations were converted to nmol L^{-1} for flux calculation.

		Net volume flux (Sv)	**Dissolved Fe (nmol L^{-1})**	**n**	**Dissolved Input**		**Particulate Fe (nmol L^{-1})**	**n**	**Particulate Input**	
					(mol y^{-1})	**(kt y^{-1})**			**(mol y^{-1})**	**(kt y^{-1})**
Central Sills Area	*< 50 m*	0.280	0.856±0.434	6	7.56±3.84 x 10^6	0.42±0.21	5.25±3.45	4	4.12±2.71 x 10^7	2.3±1.5
	> 50 m	0.413	1.66±0.478	10	2.16 x 10^7 ±6.23 x 10^6	1.2±0.35	26.2±13.5	5	3.69±1.90 x 10^8	21±11
Lancaster Sound	*< 50 m*	0.249	0.835±0.134	4	6.56±1.05 x 10^6	0.37±0.06	5.56±2.88	3	4.37±2.27 x 10^7	2.4±1.3
	> 50 m	0.447	1.37±0.416	9	1.93 x 10^7 ±5.86 x 10^6	1.1±0.33	8.71±4.42	5	1.23 x 10^8 ±6.23 x 10^7	6.8±3.5
Nares Strait[a]	*< 50 m*	0.219	-	-	5.77 x 10^6 ±9.27 x 10^5	0.32±0.05	-	-	3.84±1.99 x 10^7	2.1±1.1
	> 50 m	0.714	-	-	3.08 x 10^7 ±9.36 x 10^6	1.7±0.52	-	-	1.96 x 10^8 ±9.95 x 10^7	11±5.6
Nares Strait[b]	*< 50 m*	0.219	1.28±0.430	3	8.82±2.97 x 10^6	0.49±0.17	34.4±25.4	5	2.37±1.76 x 10^8	13±9.8
	> 50 m	0.714	3.19±1.44	9	7.18±3.24 x 10^7	4.0±1.8	48.4±18.7	4	1.09 x 10^9 ±4.22 x 10^8	61±23
Jones Sound[a]	*< 50 m*	0.003	-	-	7.90 ±1.27 x 10^4	0.004±0.001	-	-	5.26±2.73 x 10^5	0.03±0.01
	> 50 m	0.007	-	-	3.02 x 10^5 ±9.18 x 10^4	0.017±0.005	-	-	1.92 x 10^6 ±9.76 x 10^5	0.11±0.05

Iron Flux	Total Annual Input (kt y^{-1})	Bioavailable - 1.4% dissolution (kt y^{-1})[c]	Bioavailable - 54% dissolution (kt y^{-1})[c]
Atmospheric Minimum[d]	0.689	0.010	0.372
Atmospheric Maximum[e]	14.8	0.207	8.00
Lancaster Sound export[f]	10.7	1.57	6.46
Nares Strait export[f]	15.1	2.22	9.11
Nares Strait export (upper boundary)[b,f]	78.6	5.54	44
Jones Sound export[f]	0.158	0.023	0.095
CAA total - conservative estimate[f]	26	3.81	15.7
CAA total - upper boundary estimate[f]	90	7.13	50

a Dissolved and particulate Fe concentrations used to estimate Fe export from Nares Strait and Jones Sound come from the station CAA3 in Lancaster Sound.
b Dissolved and particulate Fe concentrations used to estimate Fe export from Nares Strait (upper boundary estimation) come from the station CAA1 in Lancaster Sound.
c Baker et al. (2006); **d** Marsay et al. (2018) **e** Kadko et al. (2016)
f Bioavailable Fe exported from CAA to BB is estimated by adding the dissolved Fe inventory to the particulate soluble Fe fraction, assuming a solubility range from 1.4 to 54%, as shown for bulk aerosol leaches (Baker et al., 2006).

4.4. Glacial runoff along Devon Island coast

At CAA1 station, a unique subsurface plume highly enriched in dissolved and particulate Fe, as well as pAl, pV and pMn, was present between approximately 30 to 200 m (σ_θ = 25.92-27.15; Figures 3 and 4), at the same density range where transmissivity values dropped and Chl-a increased (Colombo et al., 2019). This subsurface feature is most probably related to sediment-laden meltwater inputs from glaciers along the western side of Devon Island (Lenaerts et al., 2013; Figure 5b), which deliver extremely high loads of particulate and dissolved elements (e.g. dFe: 212 nM, pFe: 13,980, pAl: 19,355 and pMn: 151 µg L^{-1}; Colombo et al., 2019a) to CAA1 station, located 5 km offshore of the Devon coast (Figure 5b). The disproportionately high levels of pFe relative to dFe concentration (up to 3 order of magnitude higher) in glacial runoff would explain the decoupling of pFe and dFe distributions at CAA1, which do not follow the relationship described by samples collected at the other CAA stations (Figure 3b). Furthermore, the lithogenic material –glacial flour– delivered by glacial streams, is reflected in the particulate elemental to Al ratios observed in samples collected at station CAA1, which agree with UCC ratios. The lithogenic component explains the vast majority of bulk particulate concentrations, including that of pV and pMn (> 90 and 80%, respectively), which are largely controlled by non-lithogenic sources at the other CAA stations (Figure S2).

In addition to the particulate trace metal enrichment documented here, a similar glacially-derived peak of dissolved lead and Mn has been described at station CAA1 (Colombo et al., 2020; Colombo et al., 2019), and adds to the growing evidence that glacial meltwater runoff could be a significant source of Fe and other trace elements to coastal waters (Bhatia et al., 2013; Kanna et al., 2020). Baffin Bay and the Labrador Sea are surrounded by extensive glacial ice-sheets (e.g. Greenland, Ellesmere Island, Devon Island, Baffin Island), and therefore, receive large amounts of glacial meltwaters and associated trace elements (Bhatia et al., 2013; Kanna et al., 2020). A phenomenon which would likely increase with glacial retreat and associated meltwater runoff in response to climate warming.

5. Concluding remarks

The shallow (z < 600 m) and shelf dominated Canadian Arctic Archipelago (CAA) plays a central role in modulating the distribution of Fe –and other trace elements– in Arctic Waters (AW) of Pacific origin transiting from the Canada Basin to Baffin Bay and the North Atlantic Ocean (Figure 6). Iron concentrations of inflowing subsurface AW from the Canada Basin (CB-endmember; dFe: 0.469±0.039 nmol kg^{-1} and pFe: 1.41±0.902 nmol L^{-1}) significantly increase while transiting the CAA, and this high Fe signature is then exported to Baffin Bay (BB-endmember; dFe: 0.884±0.108 nmol kg^{-1} and pFe: 4.38 & 6.16 nmol L^{-1}; Figure 2a). Enhanced benthic fluxes and continental shelf-seawater interactions are most likely driving the increase of dissolved and particulate Fe as well as pAl, pV and pMn in the CAA, phenomena which are substantially enhanced east of Barrow Strait, in the central sills area, where sediment resuspension and Fe concentration are highest (Figures 5 and 6). Given the overwhelming dominance of lithogenic pFe, and the lack of relationship between pFe, dFe, dMn and non-lithogenic pMn vs. N* –a tracer of sediment denitrification processes– observed in this study, sediment resuspension and non-reductive dissolution are suggested as the main mechanisms delivering Fe to subsurface CAA waters (Figure 6). The biogeochemical cycling of Fe in the CAA greatly differs from that described in the Chukchi Sea, where reductive dissolution and oxidative scavenging shape the Fe distributions of Pacific-derived waters entering the Canada Basin (Figure 6). Past studies have identified the throughflow of Arctic Waters from the CAA to BB, and on to the Labrador Sea (LS), as an important net source of silicate and phosphate to the North Atlantic, with the latter supporting a significant fraction of nitrogen fixation (Yamamoto-Kawai et al., 2006); these macronutrients then trigger intense phytoplankton blooms in BB and LS (Hill et al., 2013; Lehmann et al., 2019; Michel et al., 2006; Varela et al., 2013). In this work, we present the first evidence of substantial Fe enrichment in transiting AW as result of enhanced sediment resuspension and dissolution in the eastern CAA, thereby supporting the large macronutrient supply. Although future research is needed (e.g. seasonal observations) to accurately establish the Fe budget exported from CAA to Baffin Bay, the back-of-the-envelope Fe flux estimation presented in this study reveals the importance of the shelf-dominated CAA as a significant source term of Fe, a limiting micronutrient for phytoplankton and diazotrophic cyanobacteria (Boyd & Ellwood, 2010; Küpper et al., 2008; Moore et al., 2009), to BB waters and downstream.

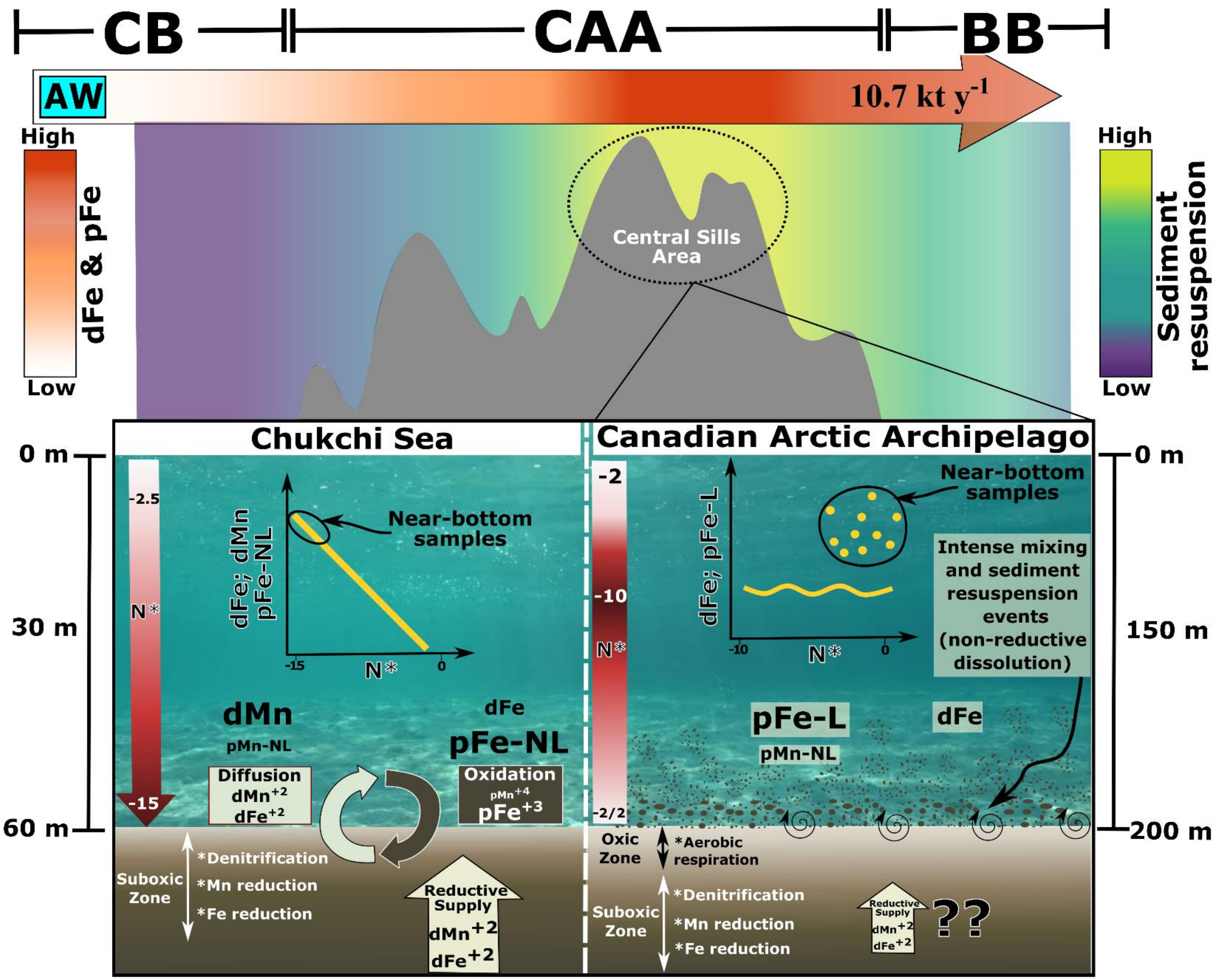

Figure 6. Conceptual scheme of the concentrations and key processes controlling the distributions of Fe in the Canadian Arctic Archipelago, in contrast with those modulating Fe in the shallow Chukchi Sea (Jensen et al., 2020; Vieira et al., 2019; Xiang & Lam, 2020). NL: Non-lithogenic fraction, L: Lithogenic fraction. The size of the text in the figure indicates the relative concentrations of Fe and Mn .

Acknowledgements

This work was supported by the Natural Sciences and Engineering Research Council of Canada (Grant NSERC-CCAR), the Northern Scientific Training Program, and by the University of British Columbia through a four-year fellowship to B.R. We thank the captain and crew of the CCGS Amundsen as well as Chief Scientist Roger Francois, PI Jay Cullen and the trace metal rosette group (Sarah Jackson, Priyanka Chandan, Kang Wang, Kathleen Munson, Jingxuan Li, David Semeniuk, Dave Janssen, Rowan Fox and Kathryn Purdon) for their assistance in sample collection. We also thank ArcticNet; Jean-Eric Tremblay's group for providing the nutrient data for the Canadian GEOTRACES 2015 cruise. The Pacific Centre for Isotopic and Geochemical Research and its staff are thanked for assistance with sample analyses. The observational data used in the resuspension analysis were accessed through the Polar Data Catalogue. Data collected during these cruises are made available by the ArcticNet science program, which is supported by the Canada Foundation for Innovation and NSERC. The particulate Arctic data reported in this study will be available in the upcoming public repositories: the GEOTRACES Intermediate Data Product 2021 via the British Oceanographic Data Centre (https://www.bodc.ac.uk/geotraces/data/idp2017/), which will be released in November 2021. Particulate trace metal data is also available in the Supporting Information document.

Research Data

The full data set of particulate Fe, Al, V, and Mn concentrations collected and discussed in this study are provided in the Supporting Information document (Table S3), along with dissolved Fe concentrations (Table S4) retrieved from Colombo et al. (2020).

Supporting Information

Tables S1-S4 and Figures S1-S4 are included in the supporting information.

Author contributions

M.C. and M.T.M. conceived the study. M.C., J.L. and K.J.O performed the sampling, and the processing and analysis of the samples. M.C. and B.R. produced the figures and statistical analyses. B.R. and S.E.A. conducted the model analysis. M.C. wrote the manuscript and M.T.M, B.R., S.E.A., J.L. and K.J.O. contributed to the discussions and manuscript writing.

Competing interests: The authors declare no competing interests

References

Abadie, C., Lacan, F., Radic, A., Pradoux, C., & Poitrasson, F. (2017). Iron isotopes reveal distinct dissolved iron sources and pathways in the intermediate versus deep Southern Ocean. *Proceedings of the National Academy of Sciences*, *114*(5), 858–863. https://doi.org/10.1073/pnas.1603107114

Aguilar-Islas, A. M., Rember, R., Nishino, S., Kikuchi, T., & Itoh, M. (2013). Partitioning and lateral transport of iron to the Canada Basin. *Polar Science*, *7*(2), 82–99. https://doi.org/10.1016/j.polar.2012.11.001

Aksenov, Y., Ivanov, V. V., Nurser, A. J. G., Bacon, S., Polyakov, I. V., Coward, A. C., et al. (2011). The arctic circumpolar boundary current. *Journal of Geophysical Research: Oceans*, *116*(9), 1–28. https://doi.org/10.1029/2010JC006637

Alkire, M. B., Jacobson, A. D., Lehn, G. O., Macdonald, R. W., & Rossi, M. W. (2017). On the geochemical heterogeneity of rivers draining into the straits and channels of the Canadian Arctic Archipelago. *Journal of Geophysical Research: Biogeosciences*, *122*(10), 2527–2547. https://doi.org/10.1002/2016JG003723

Baker, A. R., Jickells, T. D., Witt, M., & Linge, K. L. (2006). Trends in the solubility of iron, aluminium, manganese and phosphorus in aerosol collected over the Atlantic Ocean. *Marine Chemistry*, *98*(1), 43–58. https://doi.org/10.1016/j.marchem.2005.06.004

Berman-Frank, I., Cullen, J. T., Shaked, Y., Sherrell, R. M., & Falkowski, P. G. (2001). Iron availability, cellular iron quotas, and nitrogen fixation in *Trichodesmium*. *Limnology and Oceanography*, *46*(6), 1249–1260. https://doi.org/10.4319/lo.2001.46.6.1249

Beszczynska-Möller, A., Woodgate, R., Lee, C., Melling, H., & Karcher, M. (2011). A Synthesis of Exchanges Through the Main Oceanic Gateways to the Arctic Ocean. *Oceanography*, *24*(3), 82–99. https://doi.org/10.5670/oceanog.2011.59

Bhatia, M. P., Kujawinski, E. B., Das, S. B., Breier, C. F., Henderson, P. B., & Charette, M. A. (2013). Greenland meltwater as a significant and potentially bioavailable source of iron to the ocean. *Nature Geoscience*, *6*(4), 274–278. https://doi.org/10.1038/ngeo1746

Biller, D. V., & Bruland, K. W. (2014). The central California Current transition zone: A broad region exhibiting evidence for iron limitation. *Progress in Oceanography*, *120*, 370–382. https://doi.org/10.1016/j.pocean.2013.11.002

Boyd, P. W., & Ellwood, M. J. (2010). The biogeochemical cycle of iron in the ocean. *Nature Geoscience*, *3*(10), 675–682. https://doi.org/10.1038/ngeo964

Bruland, K. W., Rue, E. L., & Smith, G. J. (2001). Iron and macronutrients in California coastal upwelling regimes: Implications for diatom blooms. *Limnology and Oceanography*, *46*(7), 1661–1674. https://doi.org/10.4319/lo.2001.46.7.1661

Bruland, K. W. K., Donat, J. R. J., & Hutchins, D. A. (1991). Interactive Influences of Bioactive Trace-Metals on Biological Production in Oceanic Waters. *Limnology and Oceanography*, *36*(8), 1555–1577. https://doi.org/10.4319/lo.1991.36.8.1555

Burdige, D. J. (1993). The biogeochemistry of manganese and iron reduction in marine sediments. *Earth Science Reviews*, *35*(3), 249–284. https://doi.org/10.1016/0012-8252(93)90040-E

Carmack, E. C., & Wassmann, P. (2006). Food webs and physical-biological coupling on pan-Arctic shelves: Unifying concepts and comprehensive perspectives. *Progress in Oceanography*, *71*(2–4), 446–477. https://doi.org/10.1016/j.pocean.2006.10.004

Carrère, L., & Lyard, F. (2003). Modeling the barotropic response of the global ocean to atmospheric wind and pressure forcing - Comparisons with observations. *Geophysical Research Letters*, *30*(6), 1275–1279. https://doi.org/10.1029/2002GL016473

Charette, M. A., Kipp, L. E., Jensen, L. T., Dabrowski, J. S., Whitmore, L. M., Fitzsimmons, J. N., et al. (2020). The Transpolar Drift as a Source of Riverine and Shelf-Derived Trace Elements to the Central Arctic Ocean. *Journal of Geophysical Research: Oceans*, *125*(5), 1–34. https://doi.org/10.1029/2019JC015920

Cheize, M., Planquette, H. F., Fitzsimmons, J. N., Pelleter, E., Sherrell, R. M., Lambert, C., et al. (2019). Contribution of resuspended sedimentary particles to dissolved iron and manganese in the ocean: An experimental study. *Chemical Geology*, *511*(February), 389–415. https://doi.org/10.1016/j.chemgeo.2018.10.003

Colombo, M., Brown, K. A., De Vera, J., Bergquist, B. A., & Orians, K. J. (2019). Trace metal geochemistry of remote rivers in the Canadian Arctic Archipelago. *Chemical Geology*, *525*, 479–491. https://doi.org/10.1016/j.chemgeo.2019.08.006

Colombo, M., Rogalla, B., Myers, P. G., Allen, S. E., & Orians, K. J. (2019). Tracing Dissolved Lead Sources in the Canadian Arctic: Insights from the Canadian GEOTRACES Program. *ACS Earth and Space Chemistry*, *3*(7), 1302–1314. https://doi.org/10.1021/acsearthspacechem.9b00083

Colombo, M., Jackson, S. L., Cullen, J. T., & Orians, K. J. (2020). Dissolved iron and manganese in the Canadian Arctic Ocean: on the biogeochemical processes controlling their distributions. *Geochimica et Cosmochimica Acta*, *277*, 150–174. https://doi.org/10.1016/j.gca.2020.03.012

Conway, T. M., & John, S. G. (2014). Quantification of dissolved iron sources to the North Atlantic Ocean. *Nature*, *511*(7508), 212–215. https://doi.org/10.1038/nature13482

Covelli, S., & Fontolan, G. (1997). Application of a normalization procedure in determining regional geochemical baselines. *Environmental Geology*, *30*(1–2), 34–45. https://doi.org/10.1007/s002540050130

Cullen, J. T., Chong, M., & Ianson, D. (2009). British columbian continental shelf as a source of dissolved iron to the subarctic northeast Pacific Ocean. *Global Biogeochemical Cycles*, *23*(4), 1–12. https://doi.org/10.1029/2008GB003326

Elrod, V. A., Berelson, W. M., Coale, K. H., & Johnson, K. S. (2004). The flux of iron from continental shelf sediments: A missing source for global budgets. *Geophysical Research Letters*, *31*(12), 2–5. https://doi.org/10.1029/2004GL020216

Epstein, J.-L. (2018). *The impact of internal tide mixing parameterizations in an eddy-permitting model of the Arctic Ocean*. University of British Columbia. Retrieved from https://open.library.ubc.ca/collections/ubctheses/24/items/1.0365809

Grivault, N., Hu, X., & Myers, P. G. (2018). Impact of the surface stress on the volume and freshwater transport through the Canadian Arctic Archipelago from a high-resolution numerical simulation. *Journal of Geophysical Research: Oceans*, *123*(12), 9038–9060.

Hatta, M., Measures, C. I., Wu, J., Roshan, S., Fitzsimmons, J. N., Sedwick, P., & Morton, P. (2015). An overview of dissolved Fe and Mn distributions during the 2010-2011 U.S. GEOTRACES north Atlantic cruises: GEOTRACES GA03. *Deep-Sea Research Part II: Topical Studies in Oceanography*, *116*, 117–129. https://doi.org/10.1016/j.dsr2.2014.07.005

Hill, V. J., Matrai, P. A., Olson, E., Suttles, S., Steele, M., Codispoti, L. A., & Zimmerman, R. C. (2013). Synthesis of integrated primary production in the Arctic Ocean: II. In situ and remotely sensed estimates. *Progress in Oceanography*, *110*, 107–125. https://doi.org/10.1016/j.pocean.2012.11.005

Hioki, N., Kuma, K., Morita, Y., Sasayama, R., Ooki, A., Kondo, Y., et al. (2014). Laterally spreading iron, humic-like dissolved organic matter and nutrients in cold, dense subsurface water of the Arctic Ocean. *Scientific Reports*, *4*, 1–9. https://doi.org/10.1038/srep06775

Homoky, W. B., Weber, T., Berelson, W. M., Conway, T. M., Henderson, G. M., van Hulten, M., et al. (2016). Quantifying trace element and isotope fluxes at the ocean-sediment boundary: A review. *Philosophical Transactions of the Royal Society A: Mathematical, Physical and Engineering Sciences*, *374*(2081), 1–43. https://doi.org/10.1098/rsta.2016.0246

Hu, X., Sun, J., Chan, T. O., & Myers, P. G. (2018). Thermodynamic and dynamic ice thickness contributions in the Canadian Arctic Archipelago in NEMO-LIM2 numerical simulations. *The Cryosphere*, *12*(4), 1233–1247.

Hughes, K. G., Klymak, J. M., Hu, X., & Myers, P. G. (2017). Water mass modification and mixing rates in a 1/12° simulation of the Canadian Arctic Archipelago. *Journal of Geophysical Research: Oceans*, *122*(2), 803–820. https://doi.org/10.1002/2016JC012235

Jakobsson, M. (2002). Hypsometry and volume of the Arctic Ocean and its constituent seas. *Geochemistry, Geophysics, Geosystems*, *3*(5), 1–18. https://doi.org/10.1029/2001gc000302

Jeandel, C., & Oelkers, E. H. (2015). The influence of terrigenous particulate material dissolution on ocean chemistry and global element cycles. *Chemical Geology*, *395*, 50–66. https://doi.org/10.1016/j.chemgeo.2014.12.001

Jensen, L. T., Morton, P., Twining, B. S., Heller, M. I., Hatta, M., Measures, C. I., et al. (2020). A comparison of marine Fe and Mn cycling: U.S. GEOTRACES GN01 Western Arctic case study. *Geochimica et Cosmochimica Acta*, *288*, 138–160. https://doi.org/10.1016/j.gca.2020.08.006

Johnson, K. S., Chavez, F. P., & Friederich, G. E. (1999). Continental-shelf sediment as a primary source of iron for coastal phytoplankton. *Nature*, *398*, 697–700.

Kadko, D., Galfond, B., Landing, W. M., & Shelley, R. U. (2016). Determining the pathways, fate, and flux of atmospherically derived trace elements in the arctic ocean/ice system. *Marine Chemistry*, *182*, 38–50. https://doi.org/10.1016/j.marchem.2016.04.006

Kanna, N., Sugiyama, S., Fukamachi, Y., Nomura, D., & Nishioka, J. (2020). Iron Supply by Subglacial Discharge Into a Fjord Near the Front of a Marine-Terminating Glacier in Northwestern Greenland. *Global Biogeochemical Cycles*, *34*(10). https://doi.org/10.1029/2020gb006567

Karl, D., Michaels, A., Bergman, B., Capone, D. G., Carpenter, E. J., Letelier, R., et al. (2002). Dinitrogen fixation in the world's oceans. *Biogeochemistry*, *57–58*, 47–98. https://doi.org/10.1023/A:1015798105851

Kipp, L. E., Charette, M. A., Moore, W. S., Henderson, P. B., & Rigor, I. G. (2018). Increased fluxes of shelf-derived materials to the central arctic ocean. *Science Advances*, *4*(1), 1–10. https://doi.org/10.1126/sciadv.aao1302

Klunder, M. B., Bauch, D., Laan, P., De Baar, H. J. W., Van Heuven, S., & Ober, S. (2012). Dissolved iron in the Arctic shelf seas and surface waters of the central Arctic Ocean: Impact of Arctic river water and ice-melt. *Journal of Geophysical Research: Oceans*, *117*(1), 1–18. https://doi.org/10.1029/2011JC007133

Kondo, Y., Obata, H., Hioki, N., Ooki, A., Nishino, S., Kikuchi, T., & Kuma, K. (2016). Transport of trace metals (Mn, Fe, Ni, Zn and Cd) in the western Arctic Ocean (Chukchi Sea and Canada Basin) in late summer 2012. *Deep Sea Research Part I Oceanographic Research Papers*, *116*, 236–252. https://doi.org/10.1016/j.dsr.2016.08.010

Küpper, H., Šetlík, I., Seibert, S., Prášil, O., Šetlikova, E., Strittmatter, M., et al. (2008). Iron limitation in the marine cyanobacterium Trichodesmium reveals new insights into regulation of photosynthesis and nitrogen fixation. *New Phytologist*, *179*(3), 784–798. https://doi.org/10.1111/j.1469-8137.2008.02497.x

Kustka, A., Sañudo-Wilhelmy, S., Carpenter, E. J., Capone, D. G., & Raven, J. A. (2003). A revised estimate of the iron use efficiency of nitrogen fixation, with special reference to the marine cyanobacterium Trichodesmium spp. (Cyanophyta). *Journal of Phycology*, *39*(1), 12–25. https://doi.org/10.1046/j.1529-8817.2003.01156.x

Lam, P. J., & Bishop, J. K. B. (2008). The continental margin is a key source of iron to the HNLC North Pacific Ocean. *Geophysical Research Letters*, *35*(7), 1–5. https://doi.org/10.1029/2008GL033294

Lee, J. M., Heller, M. I., & Lam, P. J. (2018). Size distribution of particulate trace elements in the U.S. GEOTRACES Eastern Pacific Zonal Transect (GP16). *Marine Chemistry*, *201*(May 2017), 108–123. https://doi.org/10.1016/j.marchem.2017.09.006

Lehmann, N., Kienast, M., Granger, J., Bourbonnais, A., Altabet, M. A., & Tremblay, J.-É. (2019). Remote Western Arctic Nutrients Fuel Remineralization in Deep Baffin Bay. *Global Biogeochemical Cycles*, (3), 2018GB006134. https://doi.org/10.1029/2018GB006134

Lenaerts, J. T. M., Van Angelen, J. H., Van Den Broeke, M. R., Gardner, A. S., Wouters, B., & Van Meijgaard, E. (2013). Irreversible mass loss of Canadian Arctic Archipelago glaciers. *Geophysical Research Letters*, *40*(5), 870–874. https://doi.org/10.1002/grl.50214

Li, J. (2017). *Particulate trace metals & iron availability to phytoplankton in a changing Arctic Ocean*. University of British Columbia. Retrieved from //open.library.ubc.ca/collections/ubctheses/24/items/1.0348666

Madec, G., Bourdallé-Badie, R., Bouttier, P.-A., Bricaud, C., Bruciaferri, D., Calvert, D., et al. (2017). NEMO ocean engine. Notes du Pôle de modélisation. *L'Institut Pierre-Simon Laplace (IPSL)*, *27*.

Mark Moore, C., Mills, M. M., Achterberg, E. P., Geider, R. J., Laroche, J., Lucas, M. I., et al. (2009). Large-scale distribution of Atlantic nitrogen fixation controlled by iron availability. *Nature Geoscience*, *2*(12), 867–871. https://doi.org/10.1038/ngeo667

Marsay, C. M., Kadko, D., Landing, W. M., Morton, P. L., Summers, B. A., & Buck, C. S. (2018). Concentrations, provenance and flux of aerosol trace elements during US GEOTRACES Western Arctic cruise GN01. *Chemical Geology*, *502*(May), 1–14. https://doi.org/10.1016/j.chemgeo.2018.06.007

Melling, H., Francois, R., Myers, P. G., Perrie, W., Rochon, A., & Taylor, R. L. (2012). The Arctic Ocean-a Canadian perspective from IPY. *Climatic Change*, *115*(1), 89–113. https://doi.org/10.1007/s10584-012-0576-4

Melling, Humfrey, Agnew, T. A., Falkner, K. K., Greenberg, D. A., Lee, C. M., Münchow, A., et al. (2008). Fresh-water fluxes via pacific and arctic outflows across the Canadian polar shelf. In *Arctic-Subarctic Ocean Fluxes: Defining the Role of the Northern Seas in Climate* (pp. 193–247). https://doi.org/10.1007/978-1-4020-6774-7_10

Michel, C., Ingram, R. G., & Harris, L. R. (2006). Variability in oceanographic and ecological processes in the Canadian Arctic Archipelago. *Progress in Oceanography*, *71*(2–4), 379–401. https://doi.org/10.1016/j.pocean.2006.09.006

Michel, Christine, Hamilton, J., Hansen, E., Barber, D., Reigstad, M., Iacozza, J., et al. (2015). Arctic Ocean outflow shelves in the changing Arctic: A review and perspectives. *Progress in Oceanography*, *139*, 66–88. https://doi.org/10.1016/j.pocean.2015.08.007

Milne, A., Schlosser, C., Wake, B. D., Achterberg, E. P., Chance, R., Baker, A. R., et al. (2017). Particulate phases are key in controlling dissolved iron concentrations in the (sub)tropical North Atlantic. *Geophysical Research Letters*, *44*(5), 2377–2387. https://doi.org/10.1002/2016GL072314

Morton, P. L., Landing, W. M., Shiller, A. M., Moody, A., Kelly, T. D., Bizimis, M., et al. (2019). Shelf inputs and lateral transport of Mn, Co, and Ce in the western north pacific ocean. *Frontiers in Marine Science*, *6*, 1–25. https://doi.org/10.3389/fmars.2019.00591

Nielsdóttir, M. C., Moore, C. M., Sanders, R., Hinz, D. J., & Achterberg, E. P. (2009). Iron limitation of the postbloom phytoplankton communities in the Iceland Basin. *Global Biogeochemical Cycles*, *23*(3), n/a-n/a. https://doi.org/10.1029/2008GB003410

Ohnemus, D. C., & Lam, P. J. (2015). Cycling of lithogenic marine particles in the US GEOTRACES North Atlantic transect. *Deep-Sea Research Part II*, *116*, 283–302. https://doi.org/10.1016/j.dsr2.2014.11.019

Ohnemus, D. C., Auro, M. E., Sherrell, R. M., Lagerström, M., Morton, P. L., Twining, B. S., et al. (2014). Laboratory intercomparison of marine particulate digestions including Piranha: A novel chemical method for dissolution of polyethersulfone filters. *Limnology and Oceanography: Methods*, *12*(AUG), 530–547. https://doi.org/10.4319/lom.2014.12.530

Pérez-Tribouillier, H., Noble, T. L., Townsend, A. T., Bowie, A. R., & Chase, Z. (2020). Quantifying Lithogenic Inputs to the Southern Ocean Using Long-Lived Thorium Isotopes. *Frontiers in Marine Science*, *7*(April), 1–16. https://doi.org/10.3389/fmars.2020.00207

Radic, A., Lacan, F., & Murray, J. W. (2011). Iron isotopes in the seawater of the equatorial Pacific Ocean: New constraints for the oceanic iron cycle. *Earth and Planetary Science Letters*, *306*(1–2), 1–10. https://doi.org/10.1016/j.epsl.2011.03.015

Rotermund, L. M., Williams, W. J., Klymak, J. M., Wu, Y., Scharien, R. K., & Haas, C. (2021). The Effect of Sea Ice on Tidal Propagation in the Kitikmeot Sea, Canadian Arctic Archipelago. *Journal of Geophysical Research: Oceans*, *126*(5), 1–18. https://doi.org/10.1029/2020JC016786

Rudnick, R. L., & Gao, S. (2013). *Composition of the Continental Crust*. *Treatise on Geochemistry: Second Edition* (2nd ed., Vol. 4). Elsevier Ltd. https://doi.org/10.1016/B978-0-08-095975-7.00301-6

Ryan-Keogh, T. J., Macey, A. I., Nielsdóttir, M. C., Lucas, M. I., Steigenberger, S. S., Stinchcombe, M. C., et al. (2013). Spatial and temporal development of phytoplankton iron stress in relation to bloom dynamics in the high-latitude North Atlantic Ocean. *Limnology and Oceanography*, *58*(2), 533–545. https://doi.org/10.4319/lo.2013.58.2.0533

Schlosser, C., Schmidt, K., Aquilina, A., Homoky, W. B., Castrillejo, M., Mills, R. A., et al. (2018). Mechanisms of dissolved and labile particulate iron supply to shelf waters and phytoplankton blooms off South Georgia, Southern Ocean. *Biogeosciences*, *15*(16), 4973–4993. https://doi.org/10.5194/bg-15-4973-2018

Severmann, S., McManus, J., Berelson, W. M., & Hammond, D. E. (2010). The continental shelf benthic iron flux and its isotope composition. *Geochimica et Cosmochimica Acta*, *74*(14), 3984–4004. https://doi.org/10.1016/j.gca.2010.04.022

Shaw, D. M., Cramer, J. J., Higgins, M. D., & Truscott, M. G. (2008). Composition of the Canadian Precambrian shield and the continental crust of the earth. *Geological Society, London, Special Publications*, *24*(1), 275–282. https://doi.org/10.1144/gsl.sp.1986.024.01.24

Shelley, R. U., Landing, W. M., Ussher, S. J., Planquette, H., & Sarthou, G. (2018). Regional trends in the fractional solubility of Fe and other metals from North Atlantic aerosols (GEOTRACES cruises GA01 and GA03) following a two-stage leach. *Biogeosciences*, *15*(8), 2271–2288. https://doi.org/10.5194/bg-15-2271-2018

Twining, B. S., Rauschenberg, S., Morton, P. L., & Vogt, S. (2015). Metal contents of phytoplankton and labile particulate material in the North Atlantic Ocean. *Progress in Oceanography*, *137*, 261–283. https://doi.org/10.1016/j.pocean.2015.07.001

Varela, D. E., Crawford, D. W., Wrohan, I. A., Wyatt, S. N., & Carmack, E. C. (2013). Pelagic primary productivity and upper ocean nutrient dynamics across Subarctic and Arctic Seas. *Journal of Geophysical Research: Oceans*, *118*(12), 7132–7152. https://doi.org/10.1002/2013JC009211

Vieira, L. H., Achterberg, E. P., Scholten, J., Beck, A. J., Liebetrau, V., Mills, M. M., & Arrigo, K. R. (2019). Benthic fluxes of trace metals in the Chukchi Sea and their transport into the Arctic Ocean. *Marine Chemistry*, *208*(May), 43–55. https://doi.org/10.1016/j.marchem.2018.11.001

Wang, Q., Myers, P. G., Hu, X., & Bush, A. B. G. (2012). Flow constraints on pathways through the Canadian Arctic archipelago. *Atmosphere - Ocean*, *50*(3), 373–385. https://doi.org/10.1080/07055900.2012.704348

Wang, X. H. (2002). Tide-induced sediment resuspension and the bottom boundary layer in an idealized estuary with a muddy bed. *Journal of Physical Oceanography*, *32*(11), 3113–3131. https://doi.org/10.1175/1520-0485(2002)032<3113:TISRAT>2.0.CO;2

Woodgate, R. A., Aagaard, K., & Weingartner, T. J. (2005). Monthly temperature, salinity, and transport variability of the Bering Strait through flow. *Geophysical Research Letters*, *32*(4), 1–4. https://doi.org/10.1029/2004GL021880

Xiang, Y., & Lam, P. J. (2020). Size-Fractionated Compositions of Marine Suspended Particles in the Western Arctic Ocean: Lateral and Vertical Sources. *Journal of Geophysical Research: Oceans*, *125*(8), 1–33. https://doi.org/10.1029/2020JC016144

Yamamoto-Kawai, M., Carmack, E. C., & McLaughlin, F. (2006). Nitrogen balance and Arctic throughflow. *Nature*, *443*(7107), 43. https://doi.org/10.1038/443043a

Zhang, Y., Chen, C., Beardsley, R. C., Gao, G., Lai, Z., Curry, B., et al. (2016). Studies of the Canadian Arctic Archipelago water transport and its relationship to basin-local forcings: Results from AO-FVCOM. *Journal of Geophysical Research: Oceans*, *121*(6), 4392–4415. https://doi.org/10.1002/2016JC011634